CHAPTER 6

UNSTEADY MHD FLOW OF A MICROPOLAR

FLUID OVER A STRETCHING SHEET

Chapter 6

Unsteady MHD flow of a Micropolar fluid over a stretching sheet

Unsteady flow is used in a variety of devices, including reciprocating engines, pressure exchangers, hydraulic rams, and ocean wave machines. Design of chemical processing equipment, fog formation and dispersion, temperature and moisture distribution over agricultural fields and orchards of fruit trees, crop damage from freezing, food processing, and cooling towers are a few representative fields of interest where combined heat and mass transfer with chemical reaction effect plays an important role.

6.1   Introduction of the Problem

Eringen [9] initially proposed the idea of the micropolar fluid. Eringen [10] further created a generalized theory of thermo-microfluid. The majority of studies only consider steady flow over a stretching sheet, yet unexpected stretching of the sheet might result in unsteady fluid flow. Wall velocity or wall temperature fluctuations are a result of the unsteadiness. Krishna and Vajravelu [76] scrutinized the significance of the hall effect on unsteady MHD fluid flow. Reddy et al. [142], the effect of linear radiation on unsteady MHD liquid flow was investigated. Sheikholeslami et al. [90] examined heat from radiation affected the flow of an electrically conductive fluid. Kataria and Mittal [39] study effect of radiation on the MHD fluid flow over a vertical plate. El-Amin [68] studied MHD Natural convection Micropolar fluid flow. Li et al. [143] has researched fluids flow in the presence of Lorentz forces and the properties of the fluid. MHD boundary layer fluid flow and heat transfer was introduced by Das [115] via a vertical stretching sheet. Mittal and Patel [16]

developed MHD fluid Flows with the effect of nonlinear thermal radiation and heat generation. Mittal and Kataria [15] have studied in detail the impact of radiation on MHD fluid flow. Nadeem et al. [124] proposed boundary layer flow of MHD fluid over shrinking sheet. Kataria and Mittal [40] included velocity and temperature analysis of MHD fluid flow past an vertical plate in presence of Magnetic field. Impact of heat generation on MHD fluid flow over vertical sheet have been observed by Sheikholeslami et al. [89].

MHD mixed convection flow of Micropolar fluid due to stretched sheet discussed by Waqas et al. [96]. MHD Micropolar fluid flow over a shrinking sheet with heat generation/absorption effects have been discussed by Mishra et al. [122]. Kataria et al. [44] investigated an unsteady flow of MHD Micropolar fluid in presence of magnetic field. Effect of heat generation and heat absorption on flow of MHD fluid flow over an vertical sheet have been studied by Kataria and Patel [45]. Liao, S. J. [120] For the purpose of solving the governing equations, HAM was established.

6.2 Novelty of the Chapter

In this Chapter,the impact of nonlinear radiation on the mixed convection flow of unsteady Micropolar fluid over an stretching sheet considering chemical reaction. The solution to the problem encountered by using the method of Homotopy analysis

6.3 Mathematical Formulation of the Problem

Consider an unsteady two-dimensional MHD flow of an incompressible Micropolar fluid, heat and mass transfer over a vertical stretching sheet. The sheet is assumed to emerge vertically in the upward direction from a narrow slot with velocity

$$U_w\left(x,\ t\right) = \frac{ax}{1 - \alpha t}, \tag{6.3.1}$$

where both a and α are positive constants with dimension per unit time. We measure the positive x direction along the stretching sheet with the slot as the origin. We then measure the positive y coordinate perpendicular to the sheet in the outward direction toward the fluid flow. The surface temperature T_w and concentration C_w of the stretching sheet vary with the distance x from the sheet and time t as

$$T_w\left(x,\ t\right) = T_\infty + \frac{bx}{\left(1 - \alpha t\right)^2}, \quad C_w\left(x,\ t\right) = C_\infty + \frac{cx}{\left(1 - \alpha t\right)^2}, \tag{6.3.2}$$

where b, c are constants with dimension of temperature and concentration, respectively, over length. It is noted that the expressions for $U_w(x,t)$, $T_w(x,t)$, and $C_w(x,t)$ are valid only for $t < \alpha^{-1}$. We also remark that the sheet which is fixed at the origin is stretched by applying a force in the x-direction and the effective stretching rate $a/(1 - \alpha t)$ increases with time. The sheet temperature and concentration increase (reduce) if b and c are positive (negative), respectively. We assume that the radiation effect is significant in this study. The fluid properties are taken to be constant except for density variation with temperature and concentration in the buoyancy terms. Under those assumptions and the Boussinesq approximations, the governing boundary layer equations are given as:

$$\frac{\partial u}{\partial x} + \frac{\partial v}{\partial y} = 0, \tag{6.3.3}$$

$$\frac{\partial u}{\partial t} + u\frac{\partial u}{\partial x} + v\frac{\partial u}{\partial y} = \left(\frac{\mu + k}{\rho}\right)\frac{\partial^2 u}{\partial y^2} + \frac{k}{\rho}\frac{\partial G}{\partial y} + g\beta_T\left(T - T_\infty\right) + g\beta_C\left(C - C_\infty\right) - \frac{\sigma\mathcal{B}^2 u}{\rho}, \tag{6.3.4}$$

$$\frac{\partial G}{\partial t} + u\frac{\partial G}{\partial x} + v\frac{\partial G}{\partial y} = \frac{\gamma^*}{\rho j}\frac{\partial^2 G}{\partial y^2} - \frac{k}{\rho j}\left(2G + \frac{\partial u}{\partial y}\right), \tag{6.3.5}$$

$$\frac{\partial T}{\partial t} + u\frac{\partial T}{\partial x} + v\frac{\partial T}{\partial y} = \kappa\left(\frac{\partial^2 T}{\partial y^2}\right) - \frac{1}{\rho C_P}\frac{\partial q_r}{\partial y} + \left(\frac{\mu + k}{\rho}\right)\left(\frac{\partial u}{\partial y}\right)^2, \tag{6.3.6}$$

$$\frac{\partial C}{\partial t} + u\frac{\partial C}{\partial x} + v\frac{\partial C}{\partial y} = D_M\frac{\partial^2 C}{\partial y^2} + k_c\left(C - C_\infty\right), \tag{6.3.7}$$

with the appropriate boundary conditions

$$u = U_w\left(x,\ t\right),\ \ v = 0,\ \ G = 0,\ \ T = T_w\left(x,\ t\right),\ \ C = C_w\left(x,\ t\right)\ \ \text{at}\ \ y = 0, \tag{6.3.8}$$

$$u \to 0,\ \ G \to 0,\ \ T \to T_\infty,\ \ C \to C_\infty\ \ as \to \infty. \tag{6.3.9}$$

Radiative heat flux q_r is given by Rosseland [126]

$$q_r = \frac{4}{3}\frac{\sigma^*}{k^*}\frac{\partial T^4}{\partial y}, \tag{6.3.10}$$

We recommend similarity variables reconstruct the governing equations (6.3.3)-(6.3.9) into the system of ordinary differential equations,

$$\eta = \sqrt{\frac{a}{\nu\left(1 - \alpha t\right)}}y,\ \ u = \frac{ax}{1 - \alpha t}f'\left(n\right),\ \ v = -\sqrt{\frac{a}{v\left(1 - \alpha t\right)}}f\left(\eta\right), \tag{6.3.11}$$

$$G = \sqrt{\frac{a^3}{v(1-\alpha t)^3}}\, xh\left(\eta\right), \quad T = T_\infty + \frac{bx}{(1-\alpha t)^2}\theta\left(\eta\right), \quad C = C_\infty + \frac{cx}{(1-\alpha t)^2}\phi\left(\eta\right),$$

$$(6.3.12)$$

We get

$$(1+K)\, f''' + f f'' - f'^2 - \frac{A}{2}\left(2f' + \eta f''\right) + Kh' + Gr_T\theta + Gr_C\phi - M^2 f' = 0, \quad (6.3.13)$$

$$\lambda 3 h'' + f h' - f' h - \frac{A}{2}\left(3h + \eta h'\right) - K\lambda_4\left(2h + f''\right) = 0, \quad\quad (6.3.14)$$

$$\left(1 + \frac{4}{3}Rd\left((\theta_w - 1)\theta + 1\right)^3\right)\theta'' + 4Rd\left((\theta_w - 1)\theta + 1\right)^2\left(\theta_w - 1\right)\theta'^2 + Pr f\theta'$$

$$- Pr f'\theta - \frac{A}{2}Pr\left(4\theta + \eta\theta'\right) + PrEc\left(1+K\right)f''^2 = 0, \quad (6.3.15)$$

$$\frac{1}{Sc}\phi'' + f\phi' - f'\phi - K_c\phi - \frac{A}{2}\left(4\phi + \eta\phi'\right) = 0, \quad\quad (6.3.16)$$

with

$$f\left(0\right) = 0, \quad f'\left(0\right) = 1, \quad h\left(0\right) = 0, \quad \theta\left(0\right) = 1, \quad \phi\left(0\right) = 1, \quad\quad (6.3.17)$$

$$f'\left(\infty\right) = 0, \quad h\left(\infty\right) = 0, \quad \theta\left(\infty\right) = 0, \quad \phi\left(\infty\right) = 0, \quad\quad (6.3.18)$$

where $A = \dfrac{\alpha}{a}$, $K = \dfrac{\kappa}{\mu}$, $Gr_T = \dfrac{g\beta_t b}{a^2}$, $Gr_C = \dfrac{g\beta_c c}{a^2}$, $\lambda_3 = \dfrac{\gamma^*}{\mu j}$, $\lambda_4 = \dfrac{\nu\left(1-\alpha t\right)}{aj}$,

$Ec = \dfrac{U_w^2}{C_p\left(T_w - T_\infty\right)}$, $Sc = \dfrac{\nu}{D_M}$, $Rd = \dfrac{4\sigma^* T_\infty^3}{k^*\kappa}$, $\theta_w = \dfrac{T_w}{T_\infty}$.

Skin friction coefficient, wall couple stress, Nusselt number and Sherwood number in dimension form are given as

$$C_{fx} = \frac{2}{\rho U_w^2}\left[\left(\mu + k\right)\frac{\partial u}{\partial y} + kG\right]_{y=0}, \quad M_{wx} = \frac{\gamma^* a}{\nu}\left(\frac{\partial G}{\partial y}\right)_{y=0},$$

$$Nu_x = \frac{-x}{T_w - T_\infty}\left(1 + \frac{16\sigma^* T^3}{3k^*\kappa}\right)\frac{\partial T}{\partial y}_{y=0}, \quad Sh_x = \frac{-x}{C_w - C_\infty}\left(\frac{\partial C}{\partial y}\right)_{y=0}.$$

$$(6.3.19)$$

Physical measures are given by

$$Re_x^{\frac{1}{2}}Cf_x = 2\left(1+K\right)f''\left(0\right), \quad Re_x^1 M_{wx} = h'\left(0\right), \quad Re_x^{-1/2}Sh_x = -\phi'\left(0\right),$$

$$Re_x^{-1/2}Nu_x = -\left(1 + \frac{4}{3}Rd\left\{1 + \left(\theta_w - 1\right)\theta\left(0\right)\right\}^3\right)\theta'\left(0\right),$$

$$(6.3.20)$$

6.4 Solution by Homotopy Analysis Method

There is also great flexibility concerning the Homotopy analysis approach to select the initial suppositions and the auxiliary linear operators $f_0(\eta)$, $h_0(\eta)$, $\theta_0(\eta)$ and $\phi_0(\eta)$ and linear operators $\mathcal{L}_f$, $\mathcal{L}_h$, $\mathcal{L}_\theta$ and $\mathcal{L}_\phi$ are so taken as to satisfy boundary conditions of the given in equations (6.3.8)-(6.3.9).

Initial guesses are

$$f_0(\eta) = 1 - e^{-\eta}, \quad h_0(\eta) = 0, \quad \theta_0(\eta) = e^{-\eta}, \quad \phi_0(\eta) = e^{-\eta}, \tag{6.4.1}$$

with auxiliary linear operators

$$\mathcal{L}_f = \frac{\partial^3 f}{\partial \eta^3} - \frac{\partial f}{\partial \eta}, \quad \mathcal{L}_h = \frac{\partial^2 h}{\partial \eta^2} - h, \quad \mathcal{L}_\theta = \frac{\partial^2 \theta}{\partial \eta^2} - \theta, \quad \mathcal{L}_\phi = \frac{\partial^2 \phi}{\partial \eta^2} - \phi, \tag{6.4.2}$$

satisfying

$$\mathcal{L}_f\left(k_1 + k_2 e^{\eta} + k_3 e^{-\eta}\right) = 0, \quad \mathcal{L}_h\left(k_4 e^{\eta} + k_5 e^{-\eta}\right) = 0, \tag{6.4.3}$$

$$\mathcal{L}_\theta\left(k_6 e^{\eta} + k_7 e^{-\eta}\right) = 0, \quad \mathcal{L}_\phi\left(k_8 e^{\eta} + k_9 e^{-\eta}\right) = 0, \tag{6.4.4}$$

6.4.1 Convergence Analysis

Their HAM solutions converge significantly with the parameter values $\hbar_f$, $\hbar_h$, $\hbar_\theta$ and $\hbar_\phi$. The necessary curves are shown in the plots for this purpose. In this case, a HAM approximation is used to draw $\hbar$-curves. Figures 6.1 - 6.4 imply range: $-1.6 \leq \hbar_f \leq -0.4$ for the auxiliary parameter $\hbar_f$, $-3.2 \leq \hbar_h \leq -0.5$ for the auxiliary parameter $\hbar_h$, $-1.5 \leq \hbar_\theta \leq -0.5$ for the auxiliary parameter $\hbar_\theta$ and $-0.35 \leq \hbar_\phi \leq -0.1$ for the auxiliary parameter $\hbar_\phi$ respectively.

6.5 Result and Discussion

The solutions are obtained in this section using Mathematica. With the support of graphs, the obtained results are clarified. This section discusses the behaviour of several important parameters, i.e., unsteadiness parameter A, Micropolar parameter K, thermal Grashof number Gr_T, Solutal Grashof number Gr_C, Micropolar parameters λ_3, λ_4, Eckert number Ec, Schmidt number Sc, Radiation parameter Rd and temperature ratio θ_w on axial and angular velocity profiles, temperature profile and concentration profile.

Figure 6.5 emphasizes the change in the profile of the axial velocity due to the variance in the Magnetic Parameter M. For large values of the magnet parameter

M, the axial velocity profile has been found to decline. Magnetic parameter M generates large Lorentz force values that flip fluid motion to the direction of flow and gradient axial velocity gradient $f'(\eta)$. The effect on the axial velocity of the Micropolar parameter K is shown in Figure 6.6. In this figure, we note that the axial velocity $f'(\eta)$ improves with an improvement in Micropolar parameter K. In the Figure 6.7, we can see the axial velocity profile is effected by Eckert number Ec. In this Figure, we note that the axial velocity profile $f'(\eta)$ increases as the Eckert number increases. The dragging force between the fluid particles means that viscous dissipation creates heat, and then this additional fluid heat increases the boosting force, creating an increment in the fluid axial velocity profile. In Figure 6.8, the effect on the axial velocity profile $f'(\eta)$ of unsteadiness parameter A is shown. We observe that the axial velocity profile for A slows down as it goes down. The region of high speed in the atmosphere increases when the maximum rate of change and maximum speed increase simultaneously. Therefore, mechanically, we concluded that the layer extending can be used to stabilize the transition from laminar to turbulent lows of liquid. Figure 6.9 designates the influence of the unsteadiness parameter A on angular velocity profile $h(\eta)$, we note that the angular velocity profile declines as A increases. The angular velocity is also considerably impacted by the increased value of the unsteadiness parameter A. The angular velocity profile increases from zero to a peak and gradually dies to zero for any instability value to increase the value of the unsteadiness parameter.

Figure 6.10 displays the Micropolar parameter λ_4 effect on the angular velocity profile $h(\eta)$. We watch in the Figure 6.10 the angular velocity profile is reduced with large amount of Micropolar parameter λ_4. However, lowering microinertia density values means that the values of λ_4 are rising. This in turn raises the angular velocity from zero to a peak, until it slowly passes to the free-flowing angular velocity. In Figure 6.11, the influence on angular velocity $h(\eta)$ of the thermal Grashof number Gr_T is shown. The outcome of Gr_T in the event of forced pure convection is to minimize velocity relative to the effect (alternative to pure forced convection), the impact of Gr_T is recognized in this figure. Physically, the positive Gr_T produced a positive pressure gradient, which improves the fluid flow in the frontier and the negative layer Gr_T, which then slows the fluid movement. It is important to retrieve that the axial rate at the moving rate of the sheet overruns at the wall with a high value of Gr_T ($Gr_T > 5$). The angular velocity $h(\eta)$ influenced by Micropolar parameter K is exhibited in Figure. 6.12. $h(\eta)$ is raised in this figure. Owing to the importance of the vortex viscosity, the angular velocity enhances considerably. In Figure 6.13 on the temperature profile $\theta(\eta)$, the influence of the Magnetic parameter

M is encountered. A drag force called a Lorentz force is generated by employing a magnetic field that is perpendicular to a flux. With Magnetic parameter values the temperature profile improvements. Thus, with the transfer of more heat energy from the wall to the flow system the fluid temperature rises. The influence of Micropolar parameter K is exhibited in the Figure 6.14 on the fluid temperature profile $\theta(\eta)$. Temperature profile decreases to increase of K. Figure 6.15 reflects the difference of the Radiation parameter Rd on temperature profile. It shows that the temperature improvement by the advances Radiation parameter Physically, driven by the growing Radiation parameter, heat is generated by the flow of fluid, which plays an essential role in the transfer of heat.

Figure 6.16 Temperature ratio θ_w enhance on profile of temperature $\theta(\eta)$. It designates that the temperature profile declines with the high values θ_w. Figure 6.17 represents the effect on the concentration profile $\phi(\eta)$ of the unsteadiness parameter A. One of the critical parameters of the solution gradually decays with the unsteadiness parameter A. Figure 6.18 exhibits the influence of the Magnetic parameter M on concentration profile $\phi(\eta)$. With extended M, $\phi(\eta)$ rise. Figure 6.19 the impression of Schmidt number Sc on concentration profile $\phi(\eta)$ is designated. We recognize the concentration profile declines with large number of Sc. Schmidt number reveals the apparent ease of momentum transfer and mass transfer and is of great importance when the binary mass transfer of multi phase flows is estimated. In Figure 6.20, the influence on the concentration $\phi(\eta)$ of the thermal Grashof number Gr_T is displayed. Fluid concentration, with rising thermal buoyancy parameter, are reduced anywhere other than on the wall. Figure 6.21 indicates skin friction changes with increased unsteadiness parameter A. Skin friction declines for large values of parameter A. In the Figure 6.22 In wall couple stress we found the effects of unsteadiness parameter A, wall couple stress decreases, for large values of unsteadiness parameter A. Figure 6.23 has an impact of Prandtl Number Pr at Nusselt Number, and Nusselt increases with Prandtl Number Pr increasing values. From the Figure 6.24 The effect of the Sherwood number unsteadiness parameter A is evident. With increased levels of the unsteadiness parameter A, the amount of Sherwood increases. The influences of the different boundaries on the coefficient of friction of the skin are included in 6.1. Accelerates the coefficient of friction of the skin by improving the values of K, Gr_T and Gr_C. Reduces the coefficient of friction of the skin by enhancing values of A. By raising the values of A and λ_3, wall couple stress reduces and by enhancing the values of K, λ_4, the coefficient of wall couple stress raises can be seen in Table 6.2. Nusselt number improves for raising K, Pr and reducing for raising A and θ_w as per Table 6.3. Significance of A, K and Sc on

Sherwood number can be found in Table 6.4, Sherwood number grows for the broad values of A, K and decreases for the broad values of Sc.

Table 6.1: Comparison of Skin friction factor $Re_x^{\frac{1}{2}}C_{fx}$ for different values of K, A, Gr_T, Gr_C.

K	A	Gr_T	Gr_C	$Re_x^{\frac{1}{2}}C_{fx}$
0.5	0.2	0.5	0.5	0.7665378485
0.6				0.7415552839
0.7				0.7167598465
	0.3			0.8020618485
	0.4			0.8374086051
		0.6		0.7551222646
		0.7		0.7437066807
			0.6	0.7355560117
			0.7	0.7045741748

Table 6.2: Comparative analysis of $Re_x^1 M_{wx}$ for the varying values of $K, A, \lambda_3, \lambda_4$.

K	A	λ_3	λ_4	$Re_x^1 M_{wx}$
0.5	0.2	0.5	0.5	0.1376752720
0.6				0.1464666317
0.7				0.1490100931
	0.3			0.1193869354
	0.4			0.1010985988
		0.6		0.0985279579
		0.7		0.0593806439
			0.6	0.1495514008
			0.7	0.1562078877

Table 6.3: Comparative analysis of $Re_x^{-1/2}Nu_x$ for the varying values of K, A, Pr, θ_w.

K	A	Pr	θ_w	$Re_x^{-1/2}Nu_x$
0.5	0.2	7.0	0.5	3.0572785904
0.6				3.0630279065
0.7				3.0693224878
	0.3			3.0674985287
	0.4			3.0095087390
		8.0		3.1570874831
		9.0		3.2360662213
			0.6	3.0077747919
			0.7	2.9341410474

Table 6.4: Comparative analysis of $Re_x^{-1/2}Sh_x$ for the varying values of K, A, Sc.

K	A	Sc	$Re_x^{-1/2}Sh_x$
0.5	0.2	0.08	1.5570938002
0.6			1.5579306614
0.7			1.5587675226
	0.3		1.5616934214
	0.4		1.5658360226
		0.10	0.9529594685
		0.12	0.7122670553
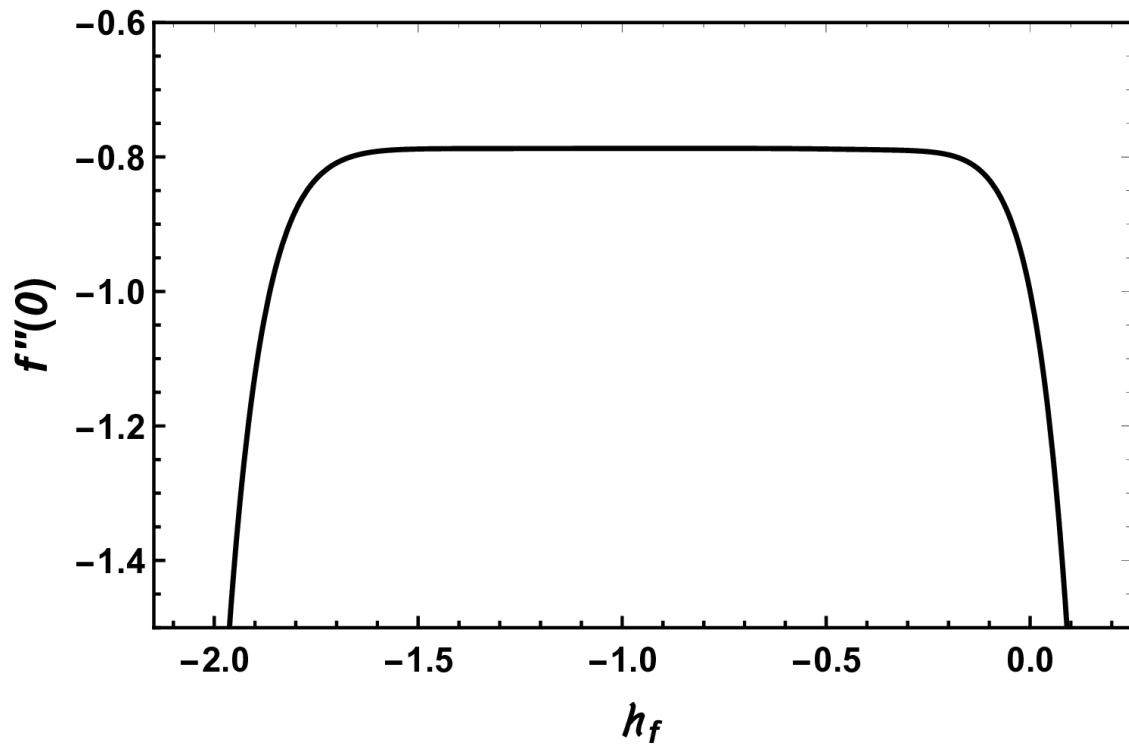
Figure 6.1: $f''(0)$ via $\hbar_f$
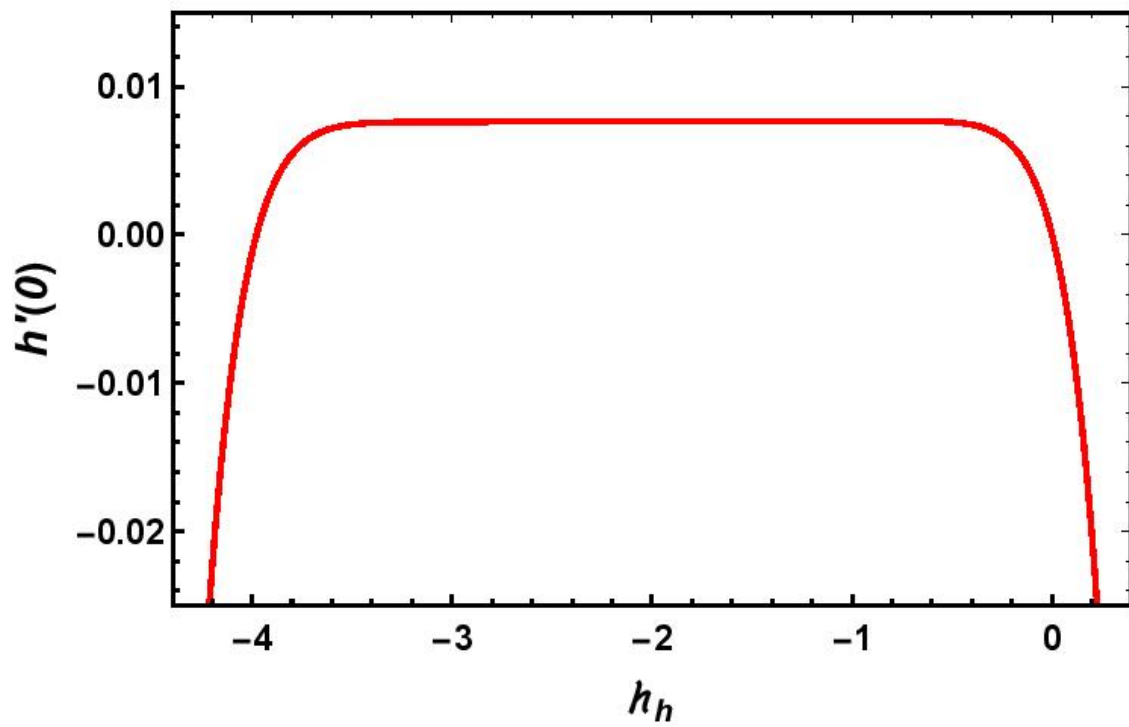
Figure 6.2: $h'(0)$ via $\hbar_h$
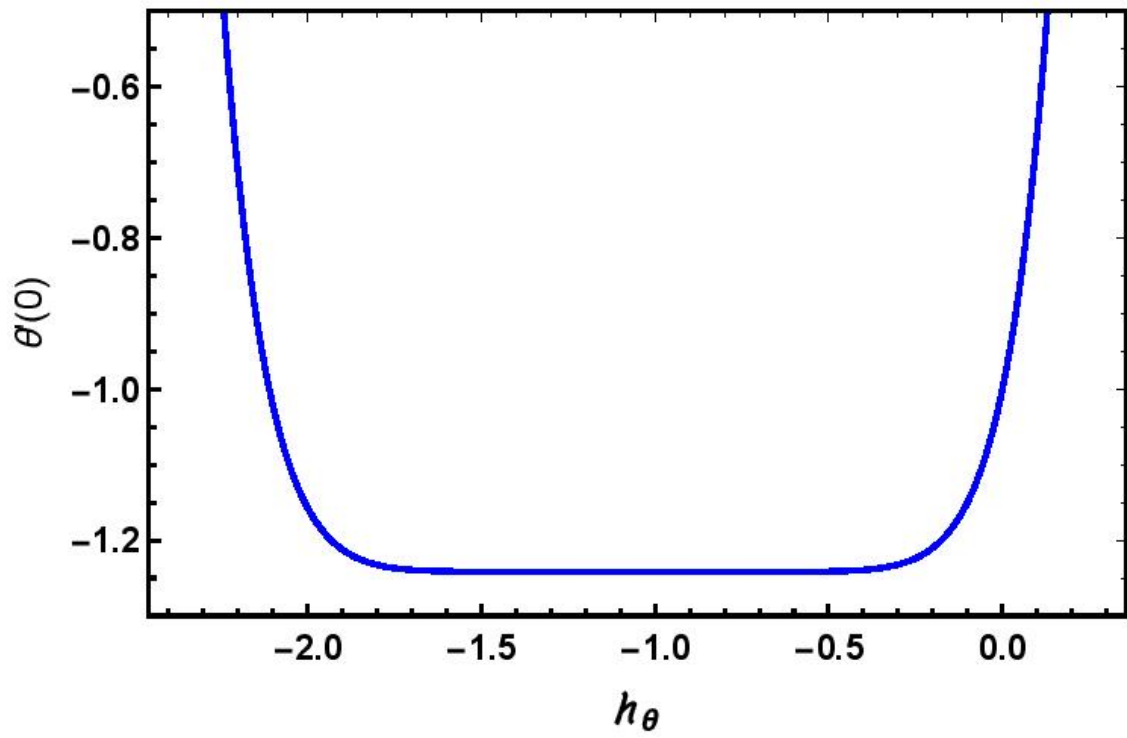
Figure 6.3: $\theta'(0)$ via $\hbar_\theta$
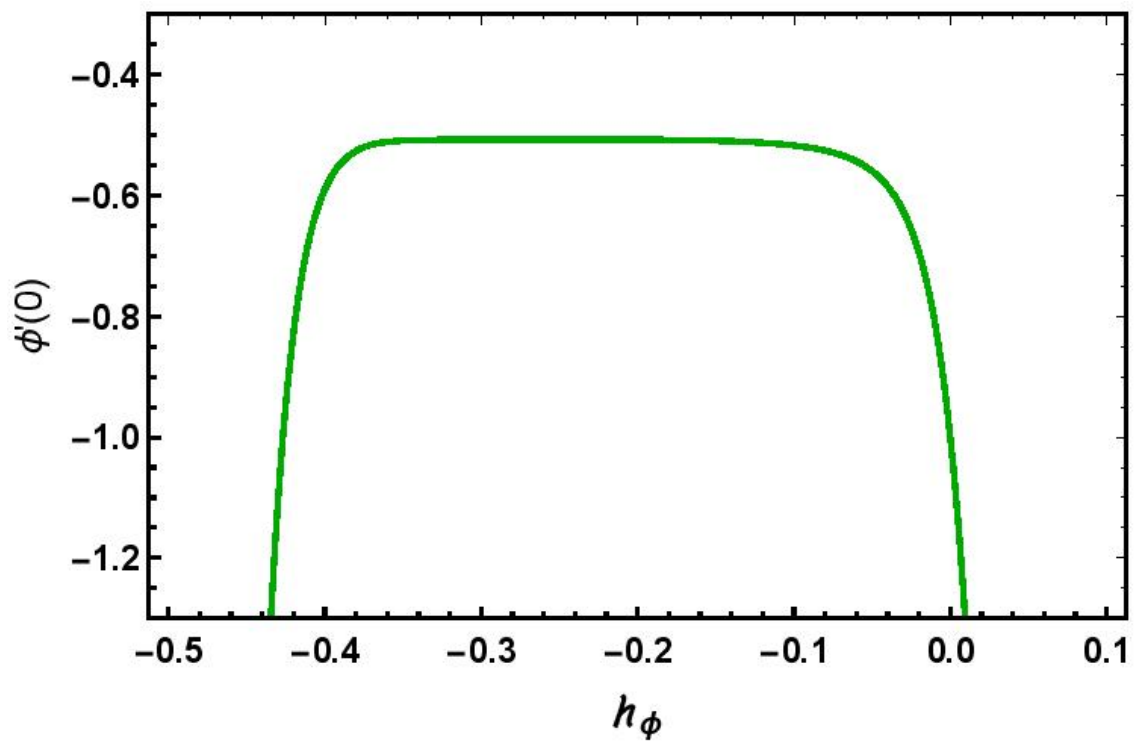
Figure 6.4: $\phi'(0)$ via $\hbar_\phi$
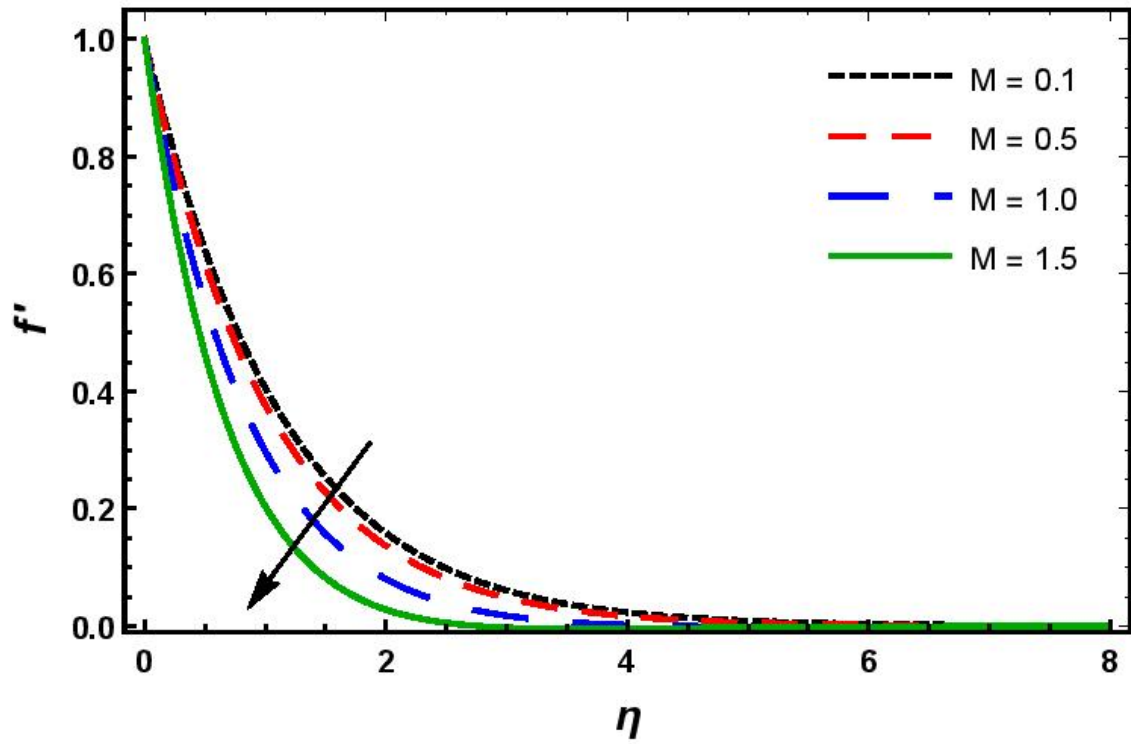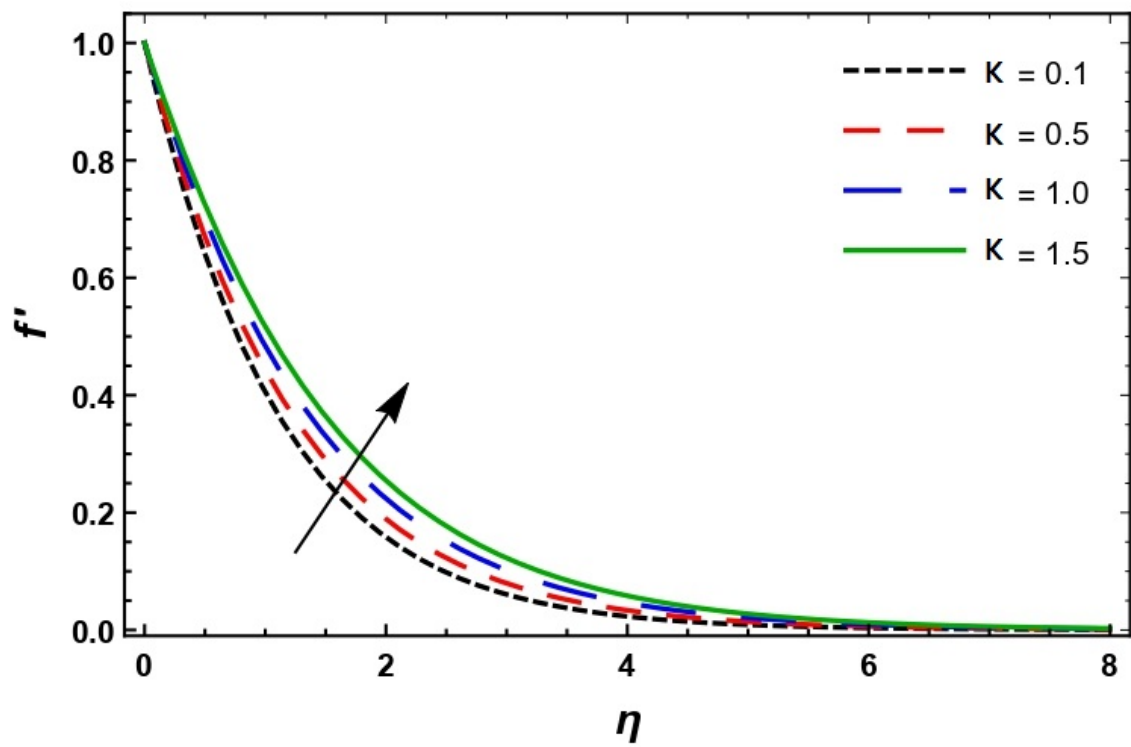
Figure 6.5: $f'(\eta)$ via M


Figure 6.6: $f'(\eta)$ via K
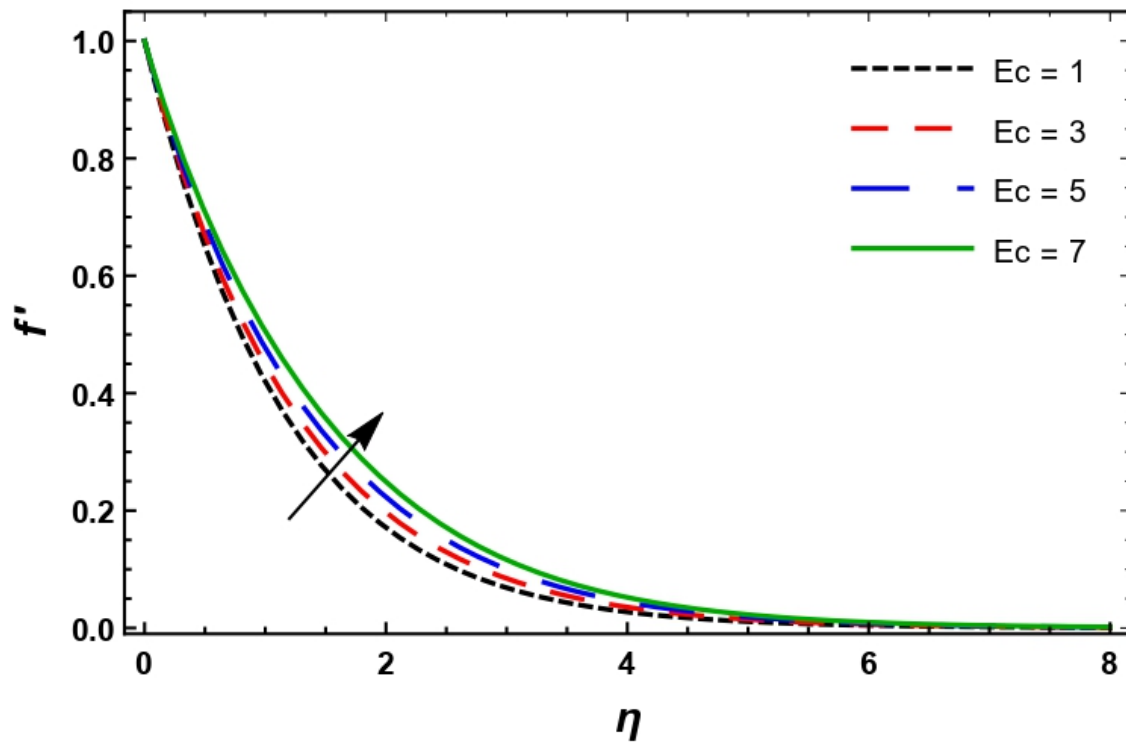
Figure 6.7: $f'(\eta)$ via Ec
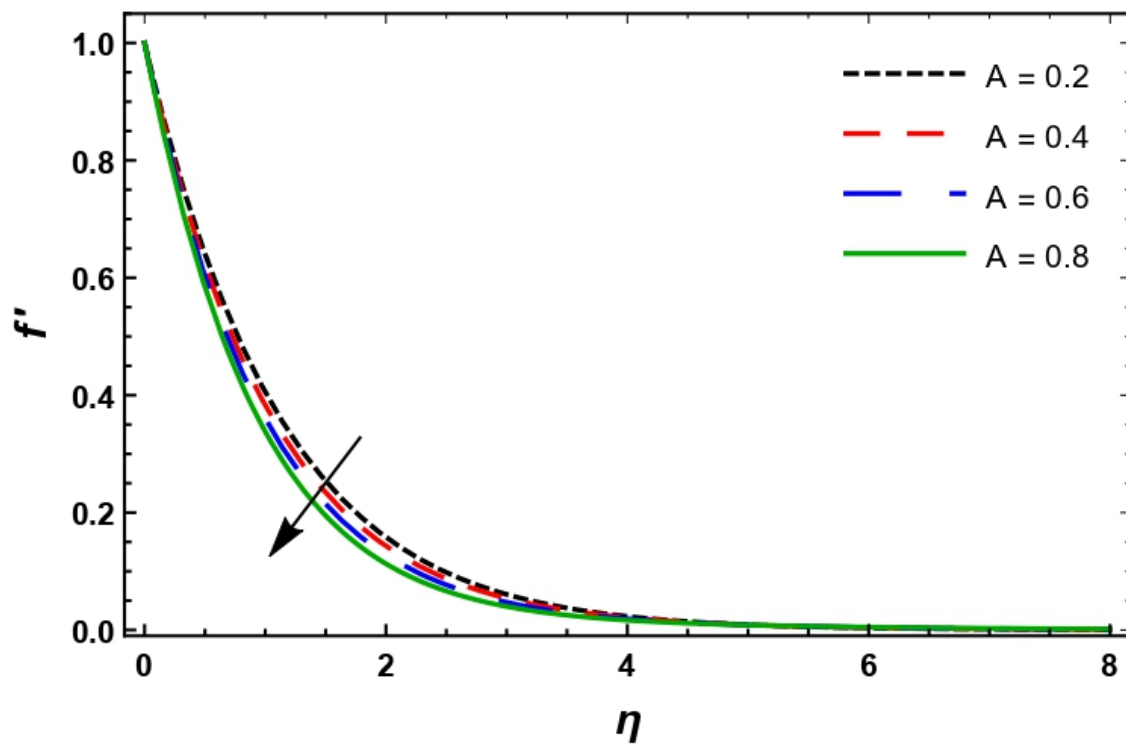
Figure 6.8: $f'(\eta)$ via A
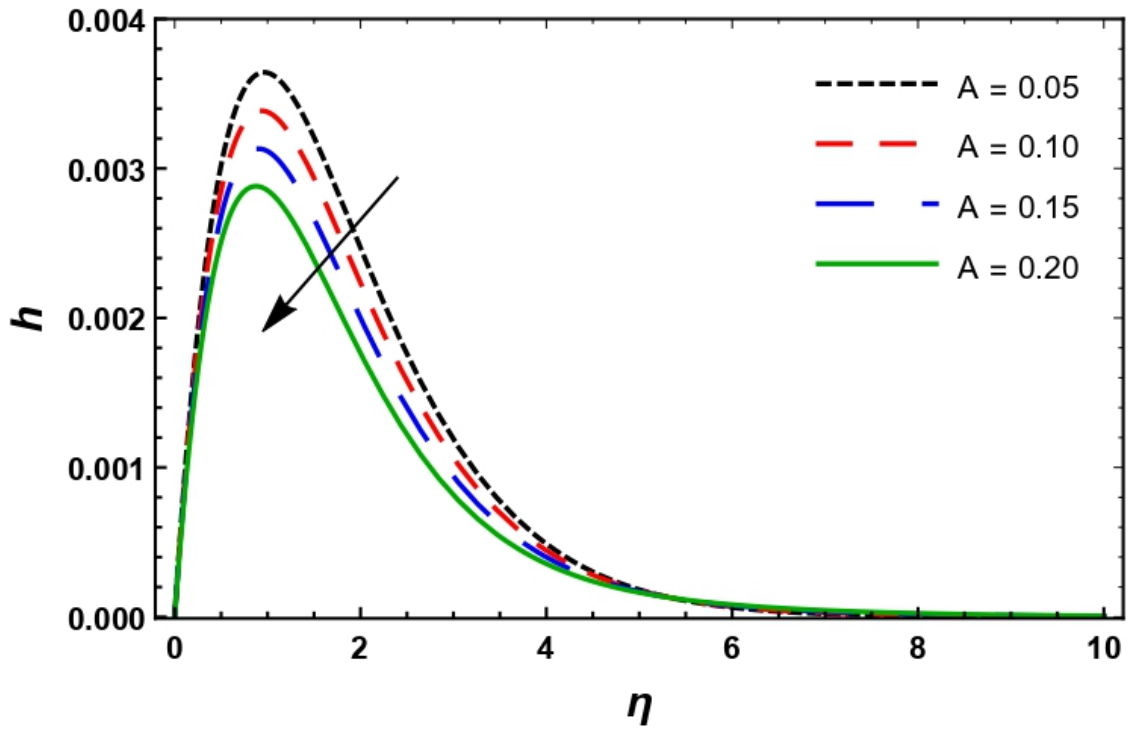
Figure 6.9: $h(\eta)$ via A
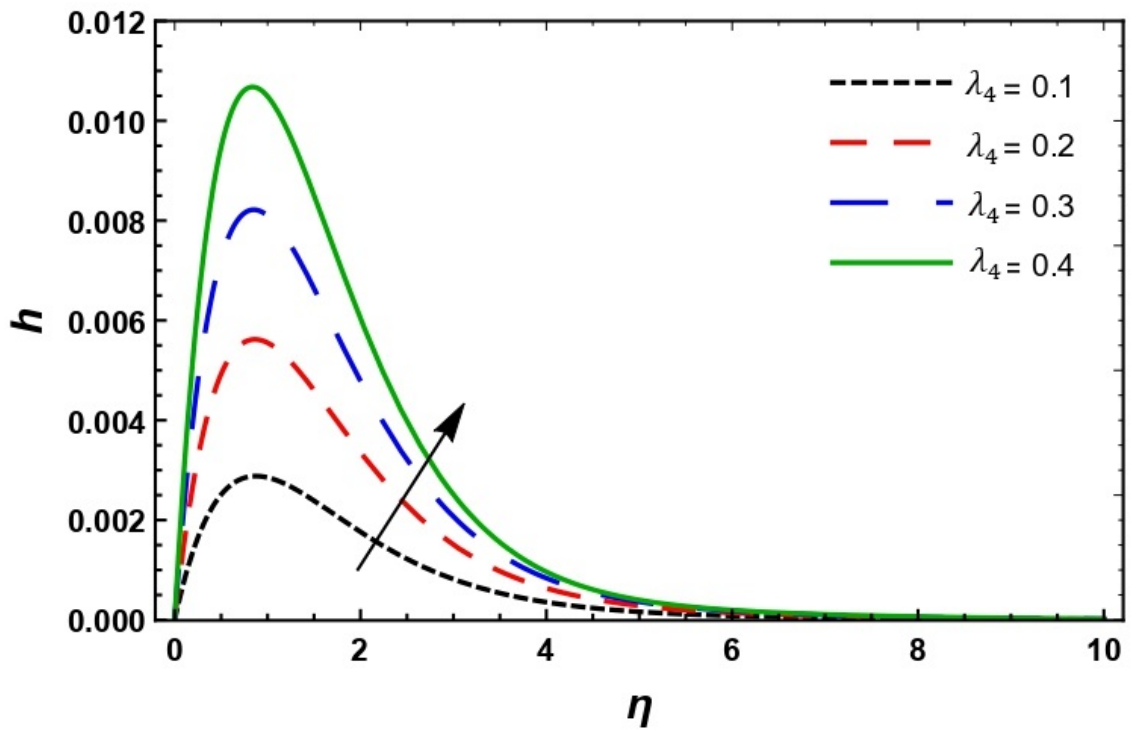

Figure 6.10: $h(\eta)$ via λ_4
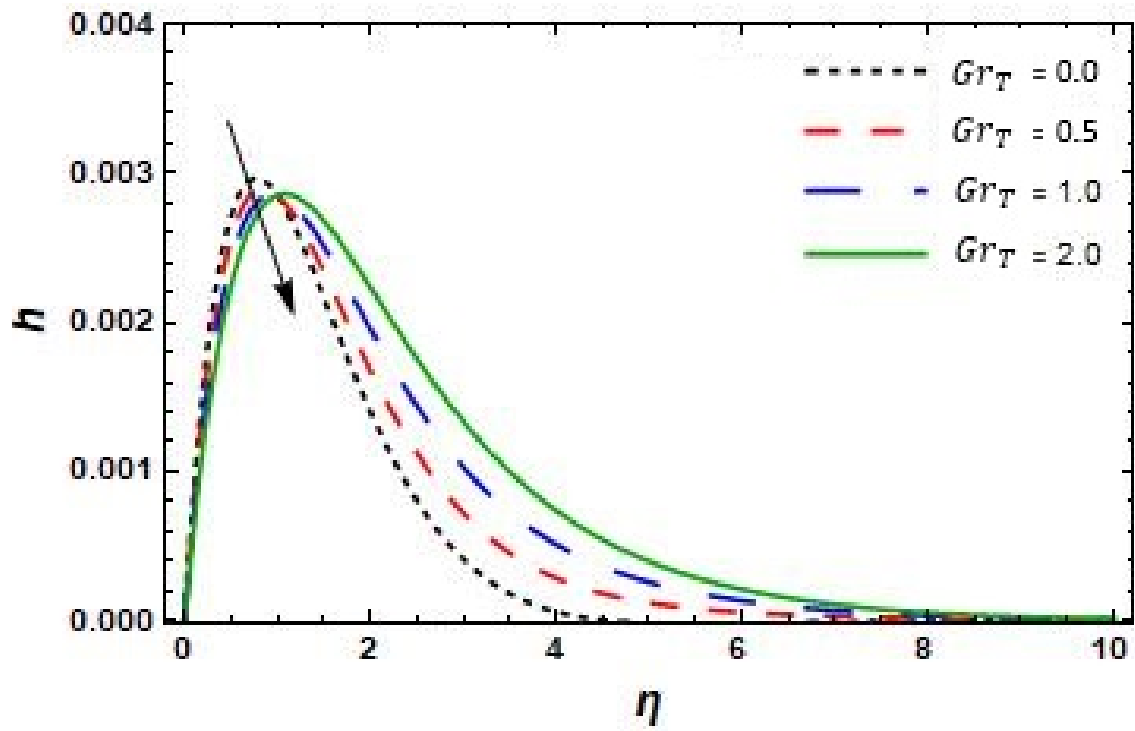
Figure 6.11: $h(\eta)$ via Gr_T
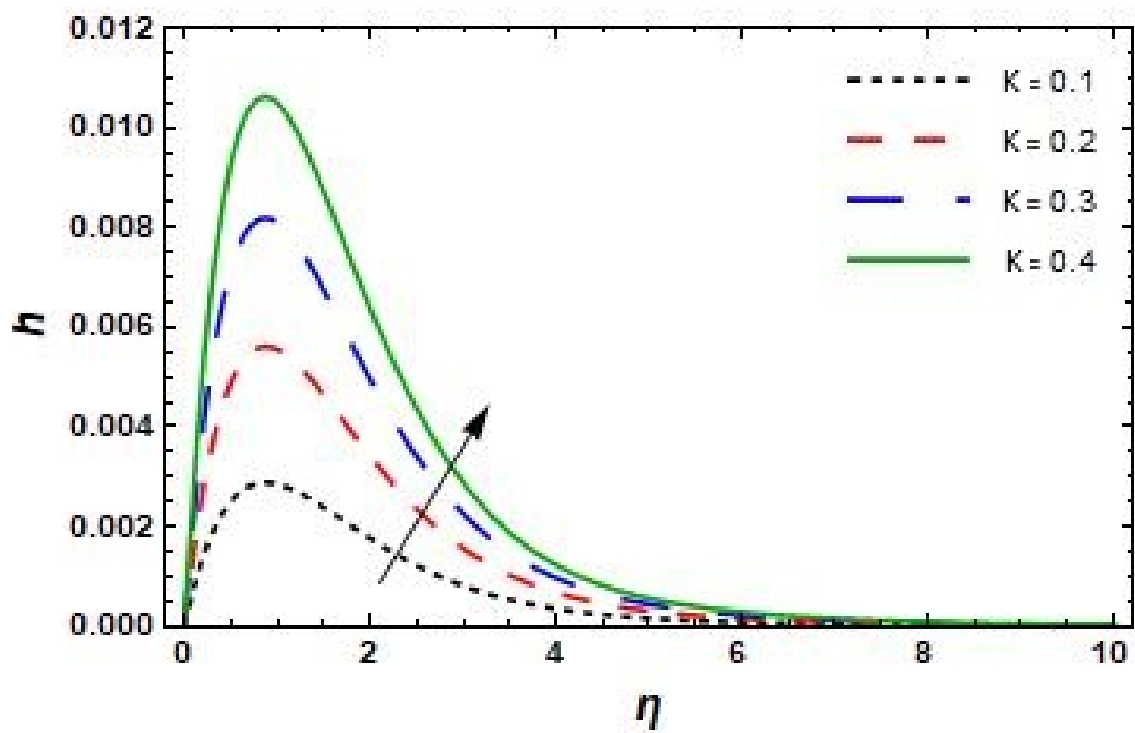
Figure 6.12: $h(\eta)$ via K
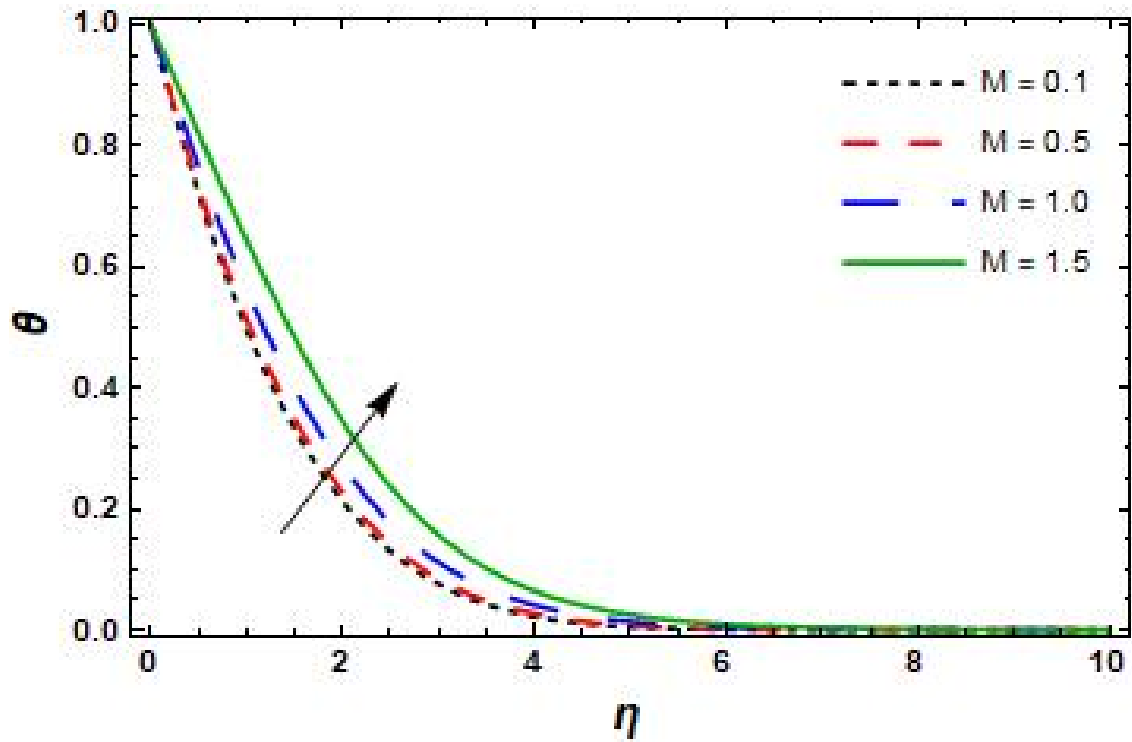
Figure 6.13: $\theta(\eta)$ via M

Figure 6.14: $\theta(\eta)$ via K

129
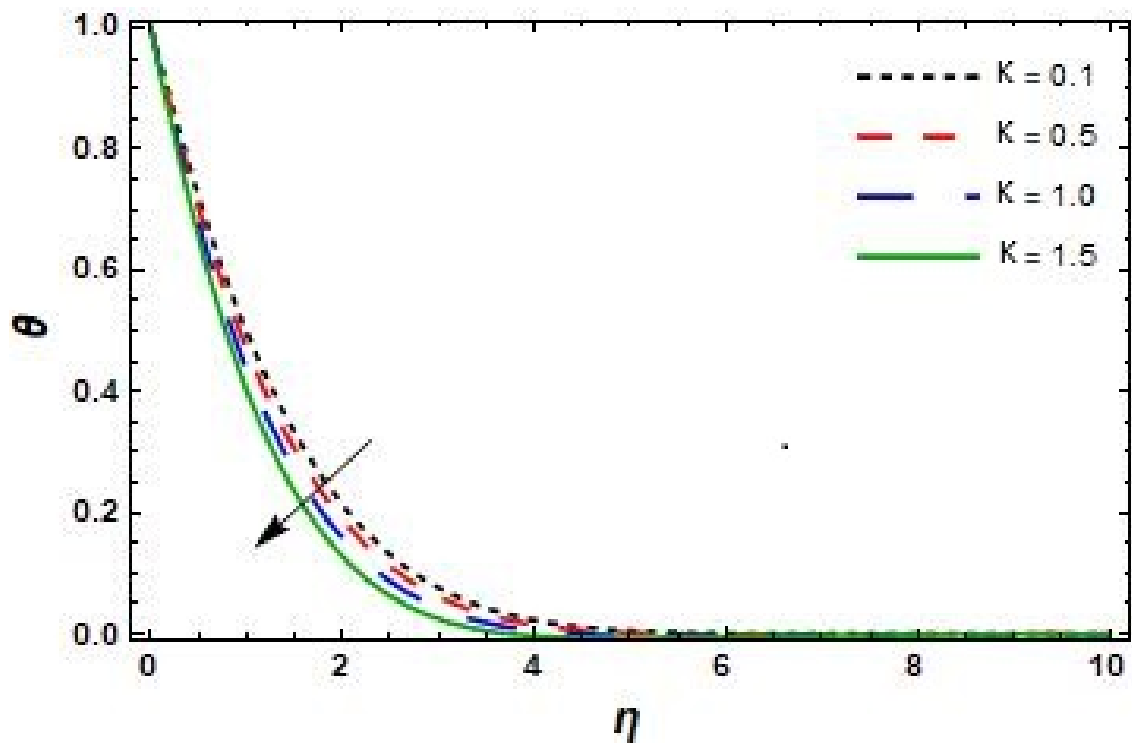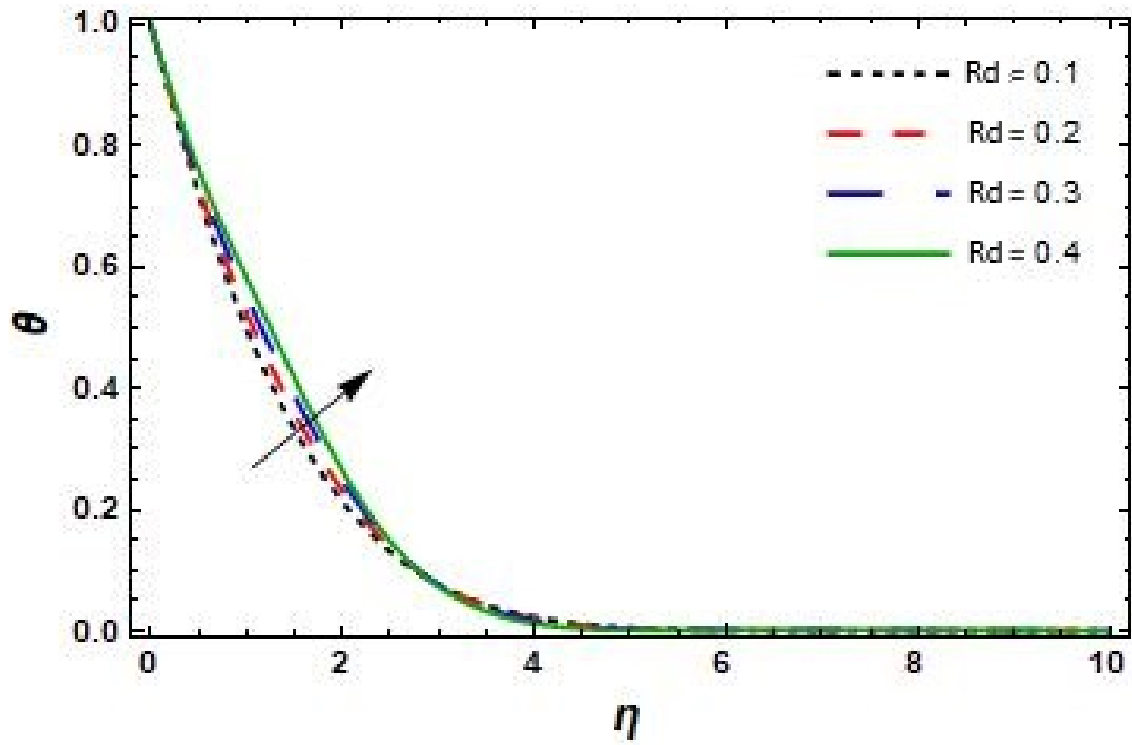
Figure 6.15: $\theta(\eta)$ via Rd
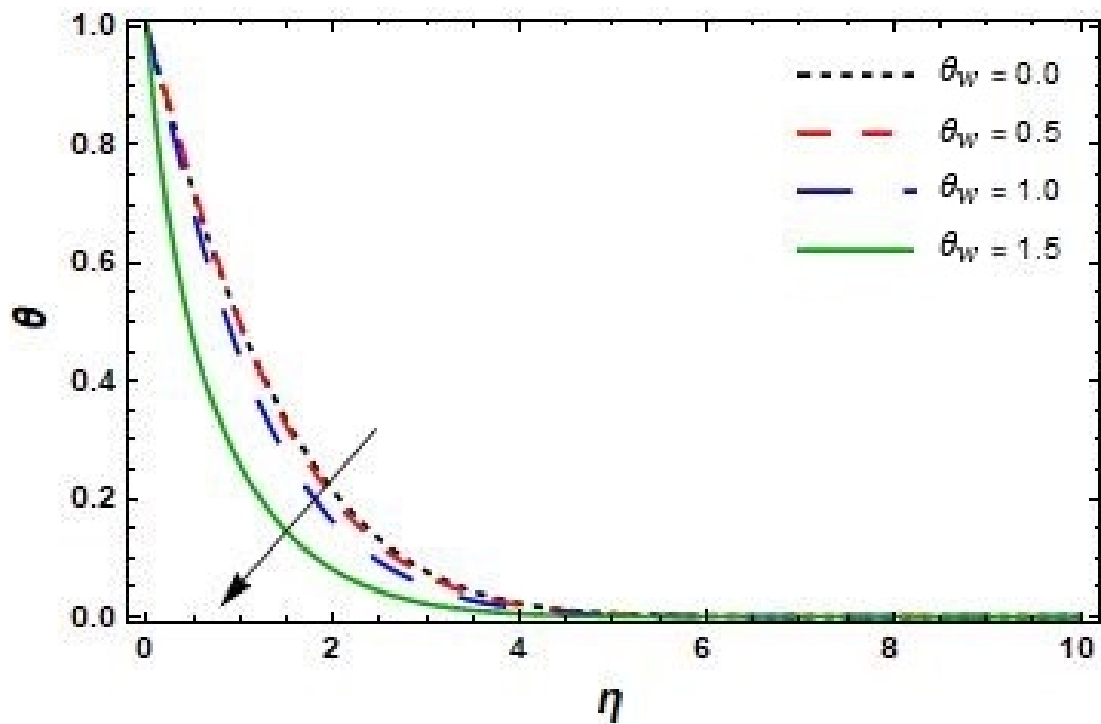
Figure 6.16: $\theta(\eta)$ via θ_w
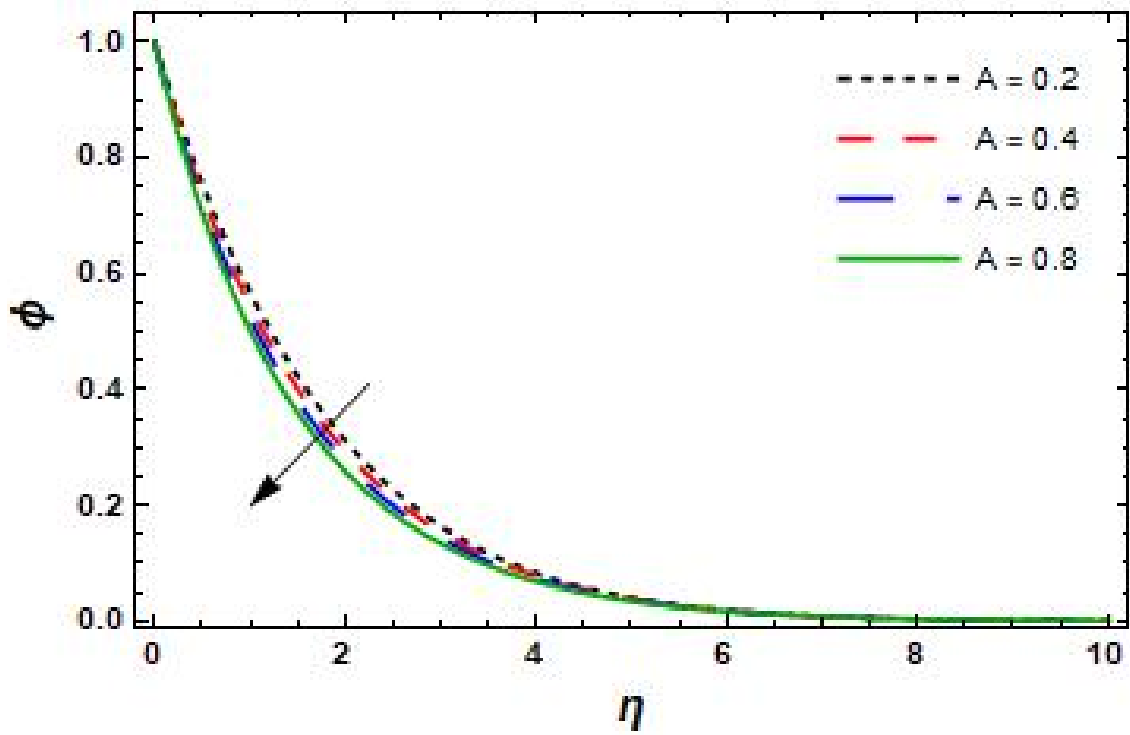
Figure 6.17: $\phi(\eta)$ via A

Figure 6.18: $\phi(\eta)$ via M

131
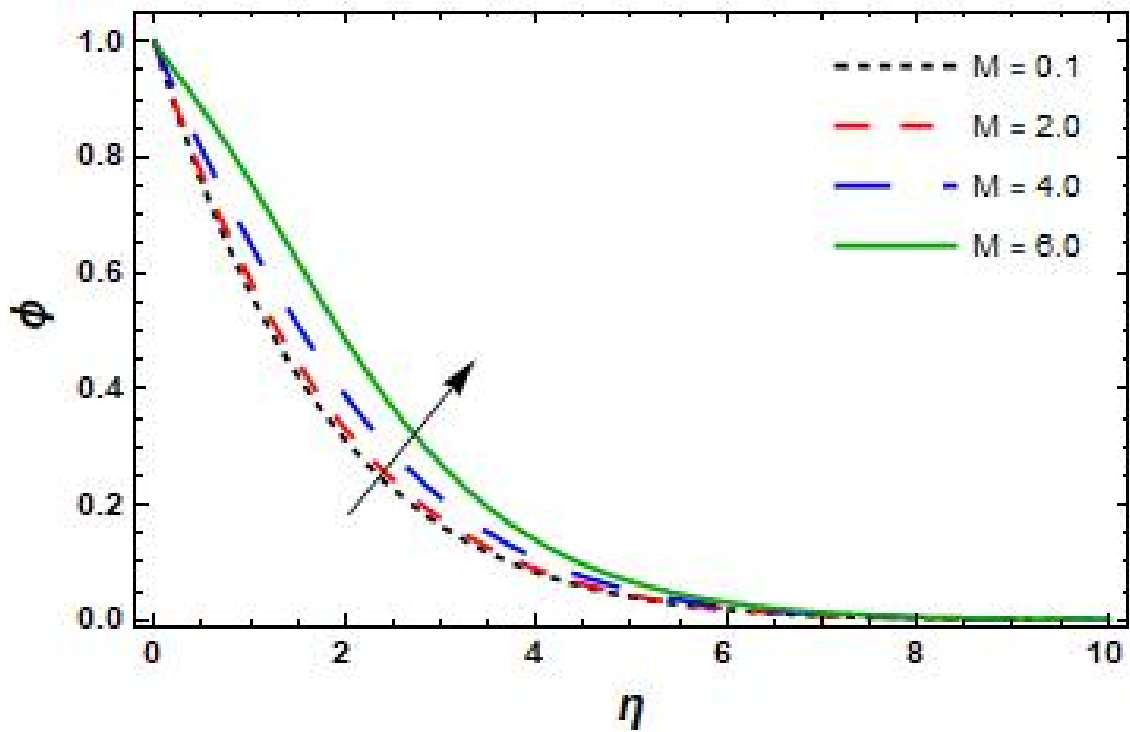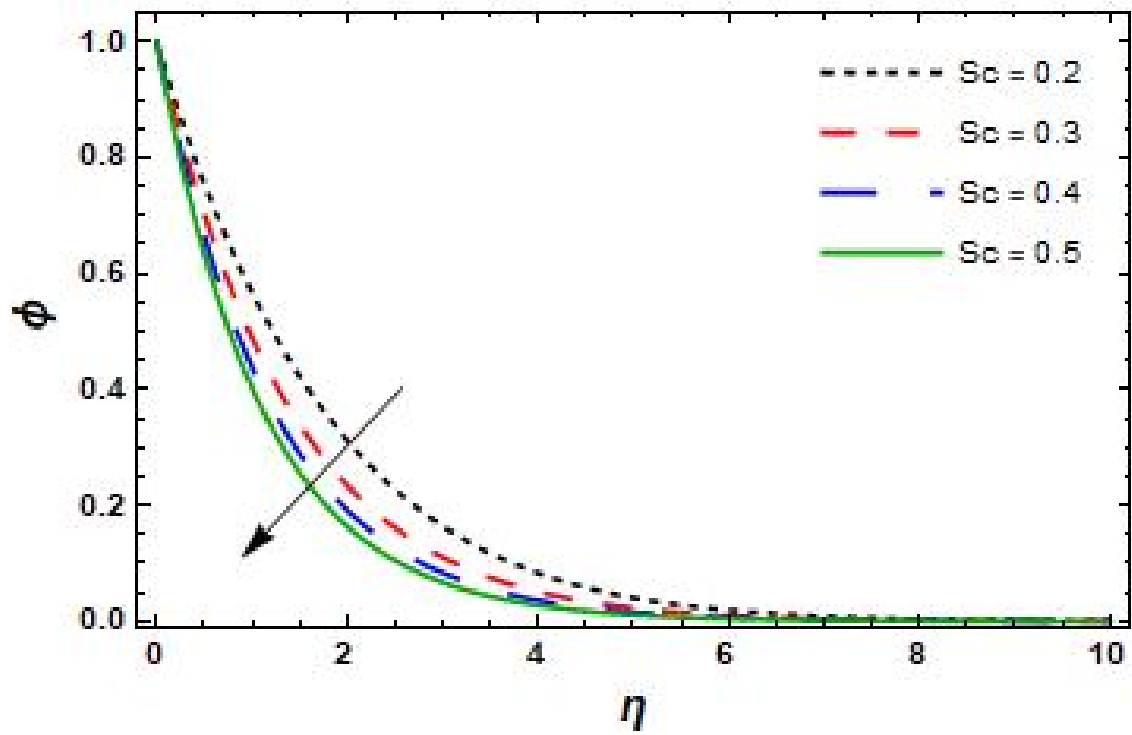
Figure 6.19: $\phi(\eta)$ via Sc
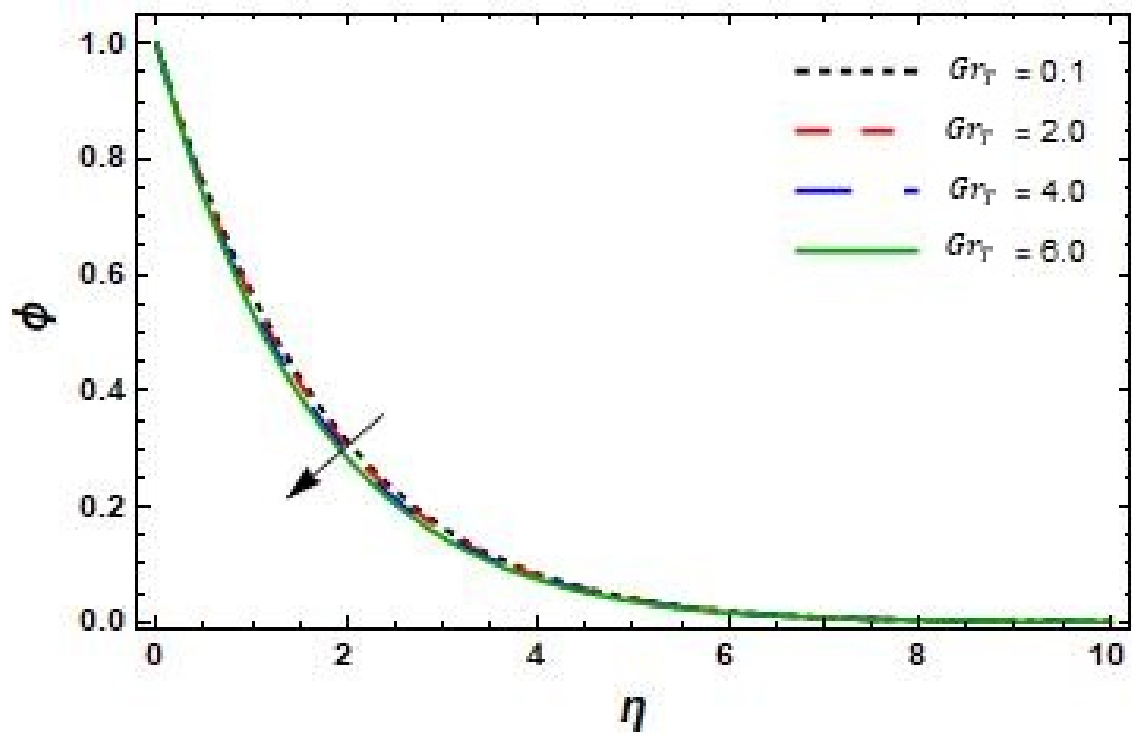
Figure 6.20: $\phi(\eta)$ via Gr_T
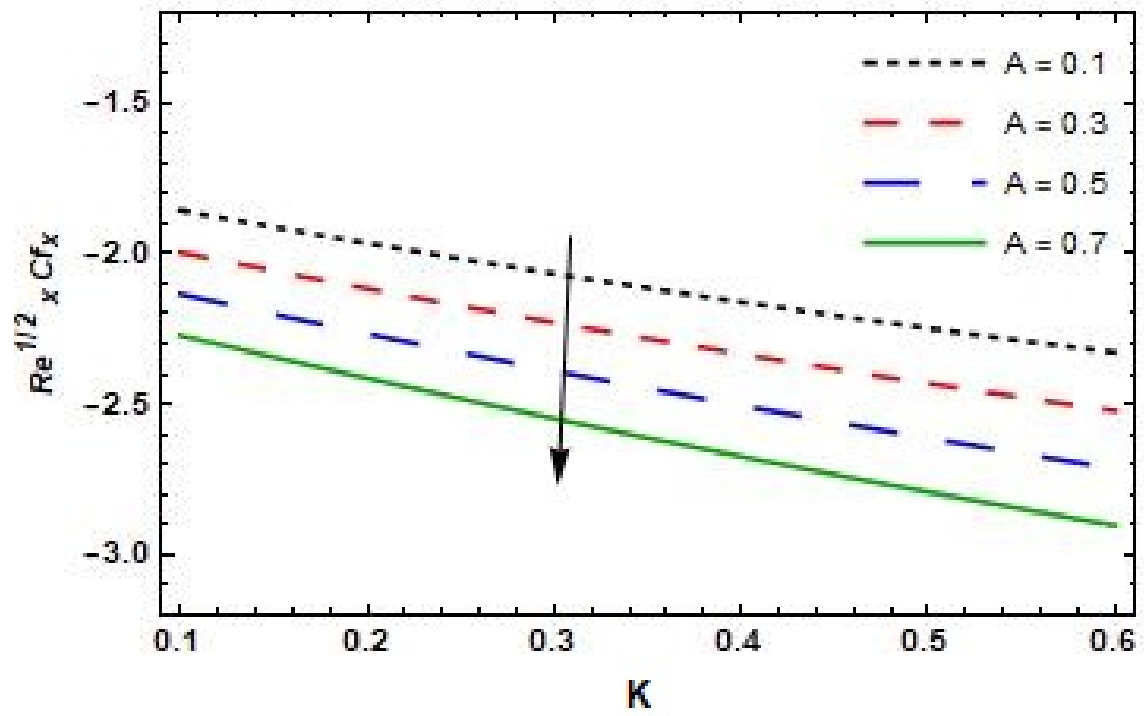
Figure 6.21: C_{fx} via A
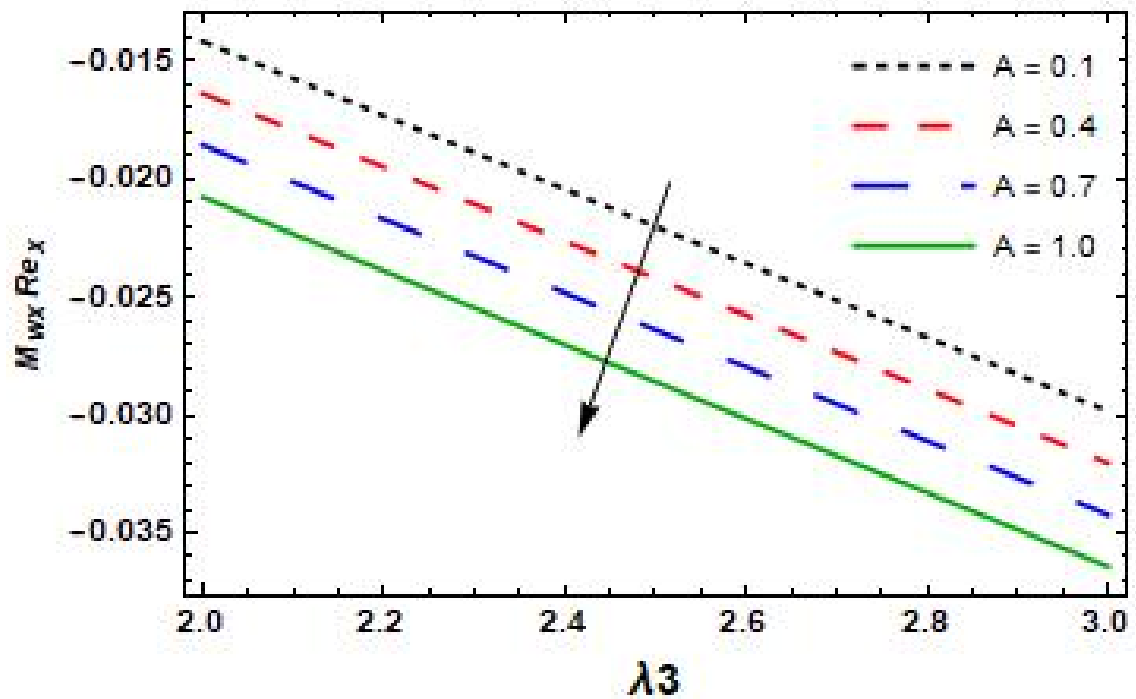
Figure 6.22: M_{wx} via A
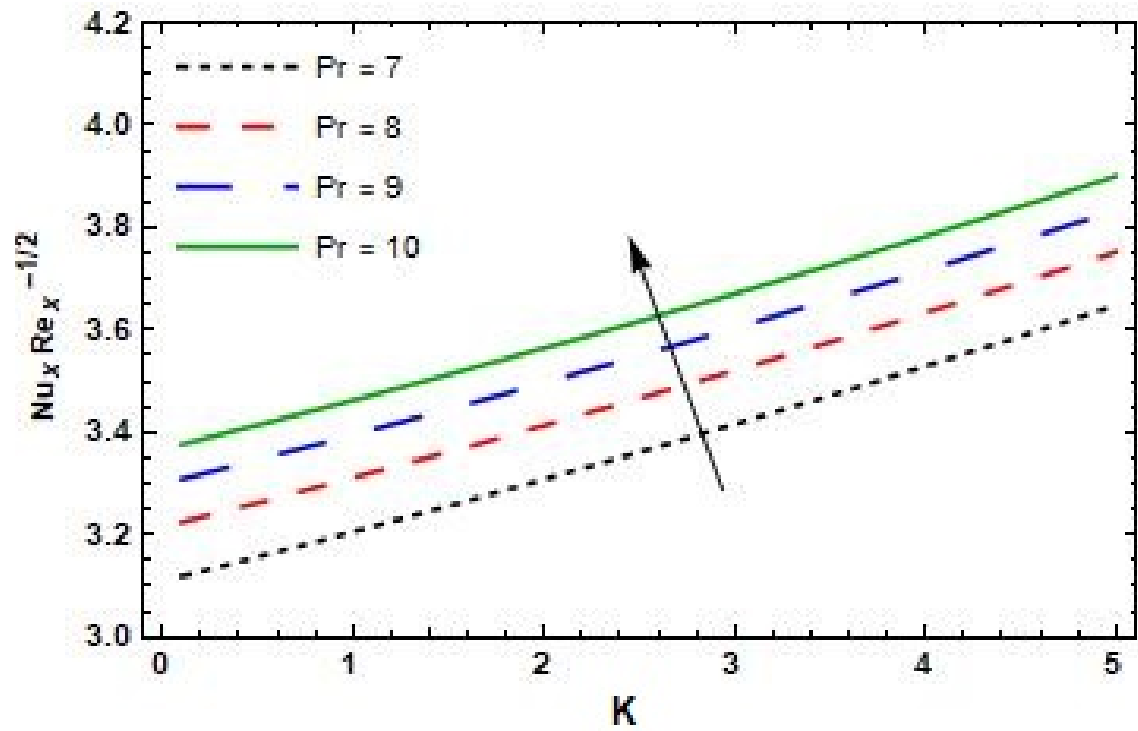
Figure 6.23: Nu_x via Pr
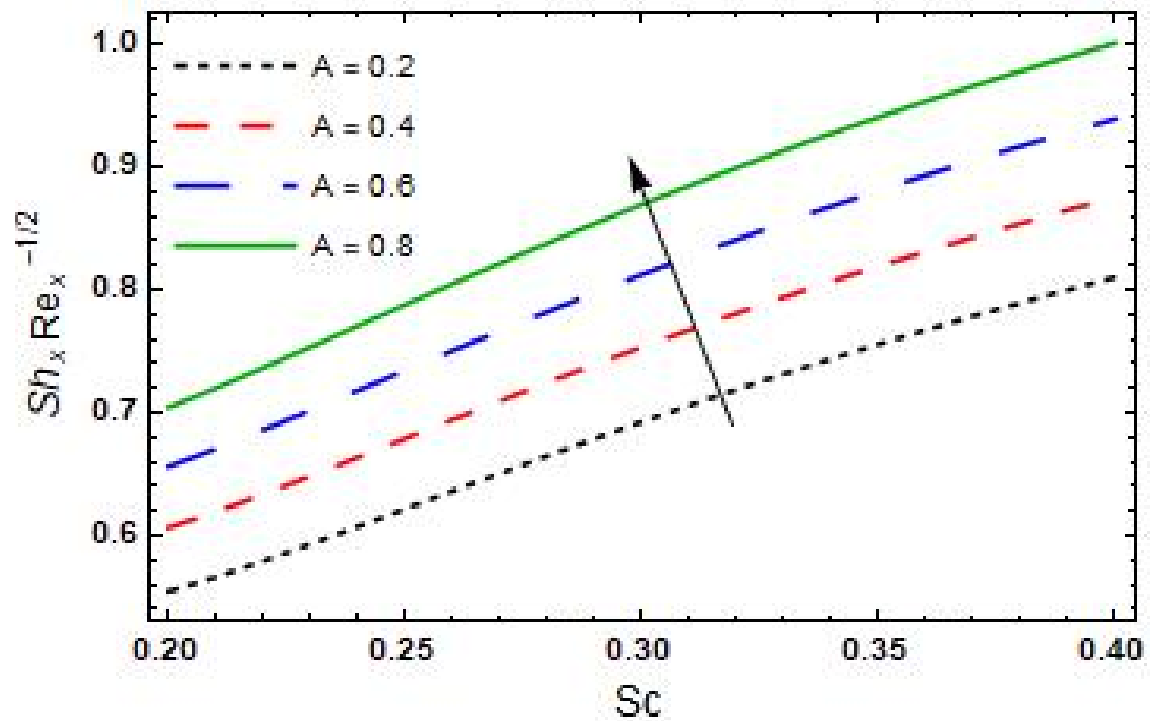
Figure 6.24: Sh_x via A

134

6.6 Conclusion

This paper examines the effects of non-linear radiation on MHD mixed convection flow of Micropolar fluid over unsteady stretching sheet accurately. By applying the method of Homotopy analysis, the dimensionless governing equations are solved. By drawing the so-called $\hbar$ -curve the convergence region of series solutions by HAM is achieved. We thought of Micropolar fluid. The results for axial velocity, angular velocity, temperature, and concentration are obtained and are graphical. The key results of this study are:

- Axial velocity profile of the Micropolar fluid declines for large values in Magnetic Parameter M and unsteadiness parameter A.

- Micropolar fluid axial velocity profile enhances for Eckert number Ec and Micropolar parameter K. The Micropolar fluid angular velocity profile enhances for broad values of Micropolar parameter K, λ_4 and declines with high values of unsteadiness parameter A and thermal Grashof number Gr_T.

- The temperature profile of the Micropolar fluid declines for high values Micropolar parameter K and Temperature ratio θ_w.

- The temperature of the object changes as it's subjected to a great magnetic field and exposure to radiation.

- For the large values of unsteadiness parameter A, thermal Grashof number Gr_T and Schmidt number Sc decreases concentration profile of the Micropolar fluid.

- For large values of Magnetic parameter M, concentration profile increases.

- Skin friction and Wall couple stress decreases for the broad unsteadiness parameter A values.

- Nusselt number increases with large amount of Prandtl number Pr.